

**Mesoporous silica nanomaterials for applications in catalysis, sensing, drug
delivery and gene transfection**

by

Daniela Rodica Radu

A dissertation submitted to the graduate faculty
in partial fulfillment of the requirements for the degree of
DOCTOR OF PHILOSOPHY

Major: Chemistry

Program of Study Committee:
Victor Shang-Yi Lin, Major Professor
William S. Jenks
Marc D. Porter
Nicola L. Pohl
Brent H. Shanks

Iowa State University


Ames, Iowa

2004

Copyright © Daniela Rodica Radu, 2004. All rights reserved.

Graduate College
Iowa State University

This is to certify that the doctoral dissertation of
Daniela Rodica Radu
has met the dissertation requirements of Iowa State University


Major Professor

For the Major Program

DEDICATION

To my children

“Float straight ahead and if the land you are looking for does not exist yet, be sure that God will create it for rewarding your courage.”

Isabella of Castile to Christopher Columbus

TABLE OF CONTENTS

LIST OF FIGURES	ix
LIST OF TABLES	xv
ACKNOWLEDGEMENTS	xvi
ABSTRACT	xvii

CHAPTER 1. GENERAL INTRODUCTION

Introduction and Dissertation Organization	1
Literature Review	4
References	7

CHAPTER 2. FINE-TUNING THE DEGREE OF ORGANIC FUNCTIONALIZATION
OF MESOPOROUS SILICA NANOSPHERE MATERIALS VIA
AN INTERFACIALLY DESIGNED CO-CONDENSATION METHOD

Abstract	11
Introduction	11
Materials and Methods	12
Results and Discussion	17
Conclusions	25
Acknowledgements	25

References	25
-------------------	----

CHAPTER 3. OXIDATIVE POLYMERIZATION OF 1,4-DIETHYNYLBENZENE
INTO HIGHLY CONJUGATED POLY(PHENYLENE BUTADIYNYLENE)
WITHIN THE CHANNELS OF SURFACE-FUNCTIONALIZED MESOPOROUS
SILICA AND ALUMINA MATERIALS

Abstract	28
Introduction	29
Materials and Methods	30
Results and Discussion	36
Conclusions	40
Acknowledgements	41
References	41

CHAPTER 4. ORGANOSULFONIC ACID-FUNCTIONALIZED MESOPOROUS
SILICAS FOR THE ESTERIFICATION OF FATTY ACIDS

Abstract	43
Introduction	44
Materials and Methods	46
Results and Discussion	49
Conclusions	59

Acknowledgements	60
References	60

CHAPTER 5. GATEKEEPING LAYER EFFECT: A POLY(LACTIC ACID)-COATED
MESOPOROUS SILICA NANOSPHERE-BASED FLUORESCENCE PROBE FOR
DETECTION OF AMINO-CONTAINING NEUROTRANSMITTERS

Abstract	63
Introduction	64
Materials and Methods	64
Results and Discussion	69
Conclusions	80
Acknowledgements	81
References	81

CHAPTER 6. REAL-TIME ATP IMAGING OF TUNABLE RELEASE FROM A
MCM-41-TYPE MESOPOROUS SILICA NANOSPHERE-BASED DELIVERY
SYSTEM

Abstract	84
Introduction	84
Materials and Methods	87
Results and Discussion	90

Conclusions	101
Acknowledgements	102
References	102

CHAPTER 7. INTRACELLULAR MESOPOROUS SILICA NANOSPHERE-BASED CONTROLLED RELEASE DELIVERY DEVICE

Abstract	106
Introduction	107
Materials and Methods	108
Results and Discussion	117
Conclusions	133
Acknowledgements	133
References	134

CHAPTER 8. A POLYAMIDOAMINE DENDRIMER-CAPPED MESOPOROUS SILICA NANOSPHERE-BASED GENE TRANSFECTION REAGENT

Abstract	137
Introduction	137
Materials and Methods	138
Results and Discussion	147
Conclusions	161

Acknowledgements	161
-------------------------	-----

References	161
-------------------	-----

CHAPTER 9. GENERAL CONCLUSIONS

General Conclusions	163
----------------------------	-----

LIST OF FIGURES

CHAPTER 1

- Figure 1-1. Schematics of MCM-41 type materials formation mechanism 5

CHAPTER 2

- Figure 2-1. Schematic representation of the synthesis of organoalkoxysilane precursors 13

- Figure 2-2. Schematic representation of the utilization of anionic organoalkoxysilane for controlling the functionalization of the MSN materials 19

- Figure 2-3. Schematic representation of the utilization of anionic organoalkoxysilane for controlling the functionalization of the MSN materials 20

- Figure 2-4. Powder XRD diffraction patterns of the MSN-SH, MSN-COOH and MSN-SO₃H (blue) materials after treatment with disulfide reducing agent (DTT) 21

- Figure 2-5. Nitrogen sorption isotherms of the MSN-SH , MSN-COOH and MSN-SO₃H materials after treatment with disulfide reducing reagent DTT and pore size distributions of the MSN-SH, MSN-COOH and MSN-SO₃H materials 21

- Figure 2-6. Solid state ¹³C CP-MAS NMR spectra of the MSN-SH, MSN-COOH, and MSN-SO₃H 22

- Figure 2-7. Schematic representation of the formation of thiol-functionalized

mesoporous silica material (MSN-SO ₃ H) via disulfide reduction with dithiothreitol (DTT)	23
CHAPTER 3	
Figure 3-1. Schematic representation of Cu ²⁺ -functionalized mesoporous silica (Cu-MCM) and alumina (Cu-MAL) catalysts for oxidative polymerization of 1,4-diethynylbenzene into conjugated oligo(phenylene butadiynylene)	30
Figure 3-2. Powder X-ray diffraction patterns of Cu-MCM before and after PPB polymerization and Cu-MAL before and after PPB polymerization	34
Figure 3-3. Absorbance measurements of polymeric material synthesized using catalysts on support or in solution	35
Figure 3-4. Nitrogen adsorption/desorption isotherms and the pore size distributions of the Cu-MCM and Cu-MAL materials before and after PPB polymerization within the mesoporous channels.	36
Figure 3-5. Normalized fluorescence emission spectra of 1,4-diethynylbenzene and the PPB-containing composite materials of Cu-MAL and Cu-MCM catalysts	37
Figure 3-6. ¹³ C CPMAS spectra of (a) structurally aligned PPB polymer catalyzed by Cu-MCM, (b) PPB polymer synthesized with Cu-MAL, and (c) bulk PPB	38
Figure 3-7. MALDI mass spectrometry measurements of the PPB polymer synthesized within the mesoporous Cu-MCM catalyst	39
CHAPTER 4	
Figure 4-1. Organosulfonic acid functional groups used in the study	49

Figure 4-2. Pore-size distribution curves for the mesoporous materials	51
Figure 4-3. Catalytic results for the esterification of palmitic acid in soybean oil with methanol	53
Figure 4-4. Effect of external mass transfer on the esterification of palmitic acid in soybean oil	55
Figure 4-5. Esterification of palmitic acid in soybean oil with methanol	58
CHAPTER 5	
Figure 5-1. Schematic representation of a surface of MSN materials: Thiol-MSN and DH-MSN	65
Figure 5-2. Schematic representation of the synthesis of PLA-coated MSN-based fluorescence sensor system for detection of amine-containing neurotransmitters	70
Figure 5-3. $^1\text{H} \rightarrow ^{13}\text{C}$ CPMAS, ^{29}Si DPMAS and $^1\text{H} \rightarrow ^{29}\text{Si}$ CPMAS spectra collected for Thiol-MSN, DH-MSN and PLA-MSN samples	73
Figure 5-4. Transmission electron micrograph (TEM) of an ultramicrotomed PLA-MSN material	74
Figure 5-5. Powder X-Ray diffraction patterns of thiol-MSN, DH-MSN, and PLA-MSN	75
Figure 5-6. BET nitrogen adsorption/desorption isotherms and BJH pore size distributions of DH-MSN and PLA-MSN materials	76
Figure 5-7. Particle size distribution and scanning electron micrographs of PLA-MSN	76
Figure 5-8. Kinetic measurements of the fluorescence detection of dopamine, tyrosine, and glutamic acid with OPTA-SS and PLA-MSN	78
Figure 5-9. HPLC chromatographs of the solution containing dopamine and glutamic	

acid before and after the introduction of PLA-MSN	79
CHAPTER 6	
Figure 6-1. SEM and TEM micrographs of PAMAM dendrimer-capped MSN	91
Figure 6-2. Solid state ^{13}C CPMAS, ^{31}P CPMAS, ^{29}Si DPMAS, and ^{29}Si CPMAS spectra of ATP-loaded MSN material capped with G2.5 PAMAM dendrimers	92
Figure 6-3. Effect of disulfide-cleaving molecules on chemiluminescence signal	94
Figure 6-4. (A) Release of encapsulated ATP from MCM-type mesoporous nanospheres	95
Figure 6-4. (B) Release of encapsulated ATP from MCM-type mesoporous nanospheres	96
Figure 6-5. Effect of uncapping agent concentration on the magnitude of release of encapsulated ATP from MCM-type mesoporous nanospheres	98
Figure 6-6. Release of encapsulated ATP from dendrimer-capped MCM-41-type mesoporous nanospheres	99
CHAPTER 7	
Figure 7-1. Schematic representation of Texas Red incorporated mesoporous silica nanospheres, T-MSN	117
Figure 7-2. Scanning electron micrographs (SEM) of the mesoporous silica nanospheres (MSN)	118
Figure 7-3. High-resolution transmission electron micrographs (TEM) of FTIC incorporate MCM-41 mesoporous silica nanospheres with amine functionality (F-MSN)	118

Figure 7-4. Schematic representation of possible interaction of MSNs with HeLa cells	120
Figure 7-5. F-MSN internalization. Dosage study and Time dependence study	121
Figure 7-6. Fluorescent MSNs after endocytosis and cell mitosis – a dividing HeLa cell	122
Figure 7-7. Cellular application of F-MSN (a) F-MSN engaged in endocytosis (b) F-MSNs inside of a HeLa cell	123
Figure 7-8. Doxorubicin delivery: Free doxorubicin delivered to HeLa Cells (a); MSN Encapsulated doxorubicin delivery in HeLa Cells (b)	124
Figure 7-9. Cleavable versus non-cleavable caps: Cells incubated with Dox-MSNs and Cells incubated with Dox-ISP-MSNs	125
Figure 7-10. HPLC study of Doxorubicin release from Dox-MSNs	127
Figure 7-11. Kinetic study of Doxorubicin release	127
Figure 7-12. Transfection of neural glia (astrocytes) with pEGFP utilizing G2-MSN as a transfection vector	130
Figure 7-13. TEM micrograph of cotransfected HeLa cells	131
Figure 7-14. Confocal fluorescence images and phase contrast images of HeLa cells (a) and CHO cells(b)	132
Figure 7-15. Relative transfection efficiencies between several transfection reagents	133
CHAPTER 8	
Figure 8-1. Schematic representation of a non-viral gene transfection	138
Figure 8-2. Schematic representation of a non-viral gene transfection system based on a Texas Red. (TR)-loaded, G2-PAMAM dendrimercapped MSN material complexed with an enhanced green fluorescence protein (<i>Aequorea victoria</i>) plasmid DNA (pEGFP-C1)	147

Figure 8-3. Powder X-Ray diffraction patterns of purified ICP-MSN, G2-MSN, and Texas Red-loaded G2-MSN materials	149
Figure 8-4. BET nitrogen adsorption/desorption isotherms	150
Figure 8-5. ^{13}C solid state CP-MAS NMR spectra of the ICP-MSN and G2-MSN materials	151
Figure 8-6. SEM (a) and TEM (300 kV) micrographs of the G2-MSN (b)	152
Figure 8-7. Complexation of G2-MSN with pEGFP-C1 DNA –electrophoresis study	153
Figure 8-8. Electrophoretic gel shifts of stability Studies of pEGFP-C1 DNA and G2-MSN-DNA Complex after Bam H1 treatment	154
Figure 8-9. Fluorescent microscopy images of HeLa cells treated with G2-MSN-DNA	154
Figure 8-10. Flow cytometry analysis of the transfection of pEGFP in HeLa cells with G2-MSN	156
Figure 8-11. Fluorescence confocal micrographs of cells transfected by pEGFP-C1-coated G2-MSN system	157
Figure 8-12. TEM micrographs of G2-MSN-DNA complexes (black dots) endocytosed by Chinese hamster ovarian (CHO) (a), human cervical cancer (HeLa) (b), and neural glia (astrocytes) (c) cells	158,159
Figure 8-13. Cell growth of (a) HeLa and (b) CHO cells in the presence of G2-MSN and in the absence of G2-MSN	160

LIST OF TABLES

Table 2-1. Structural properties of the organically functionalized MSN materials	22
Table 2-2. Elemental Analysis of the organically functionalized MSNs	24
Table 3-1. Powder XRD structural parameters of the series of Cu ²⁺ -materials	35
Table 4-1. Textural properties of the functionalized mesoporous silicas	51
Table 4-2. Comparison of the kinetic performance of the functionalized mesoporous silica catalysts	59
Table 5-1. Summary of ¹³ C CPMAS NMR data	72
Table 5-2. Summary of ²⁹ Si CPMAS NMR DATA	72
Table 5-3. Powder X-Ray diffraction results	75
Table 5-4. Nitrogen sorption isotherms	76
Table 5-5. HPLC analysis of dopamine and glutamic acid before and after the introduction of PLA-MSN	80
Table 6-1. Characteristics of release of encapsulated ATP from CdS-capped MCM-type mesoporous nanospheres for various reducing agents	100
Table 8-1. Powder X-Ray diffraction patterns	149
Table 8-2. BET and BJH parameters	150
Table 8-3. Transfection efficiency of different transfection reagents on HeLa cells	155

ACKNOWLEDGEMENTS

I would like to express my appreciation for the whole support that I have received over the past few years from so many wonderful people.

Most importantly, I would like to express my gratitude and high appreciation to my supervisor, Professor Victor Shang-Yi Lin, for his commitment to guiding me through my doctoral research, for his wisdom, for his brilliant ideas and above all this, for his mentoring.

I am much indebted to my POS Committee members, Dr. William Jenks, Dr. Marc Porter, Dr. Nicola Pohl, and Dr. Brent Shanks, in no particular order, for having accepted to be with me through this trip and helping me with their excellent suggestions.

Many thanks to Dr. Janice Buss for her suggestions and friendship.

To my family, that tolerated my absence for such a long time, my forever worship.

Finally, I am expressing my special thanks to Dr. Cheng-Yu Lai, who brought color and inspiration to all this work.

The United States Government has assigned the DOE Report number **IS-T 2497** to this thesis.

Notice: This document has been authored by the Iowa State University of Science and Technology under Contract No. W-7405-ENG-82 with the U.S. Department of Energy. The U.S. Government retains a non-exclusive, paid-up, irrevocable, world-wide license to publish or reproduce the published form of this document, or allow others to do so, for U.S. Government purposes.

ABSTRACT

Structurally well-defined mesoporous silica materials, such as MCM-type silicas with tunable pore size and narrow pore-size distribution have attracted much attention for their potential applications in adsorption, catalysis, separation, and sensing. Organofunctionalized MCM-41 silica pores could serve as synthetic scaffolds to mimic enzyme or antibody active sites for specific covalent and/or noncovalent interactions with target molecules. Herein, we designed and synthesized a fluorescence sensory system to study the molecular recognition events of biogenic molecules, such as dopamine and glucosamine, inside different functionalized mesoporous silica microenvironment.

We have also synthesized a poly(lactic acid) coated MCM-41-type mesoporous silica nanosphere (PLA-MSN) material that can serve as a fluorescence sensor system for the detection of amino-containing neurotransmitters in neutral aqueous buffer. Utilizing the PLA layer as a gatekeeper, we investigated the molecular recognition events between several structurally simple neurotransmitters, i.e., dopamine, tyrosine, and glutamic acid and a pore surface-anchored *o*-phthalic hemithioacetal (OPTA) groups. These OPTAs function as a fluorescence-sensing group that can react with the neurotransmitters with primary amine groups and form the corresponding fluorescent isoindole products. The poly(lactic acid) layer of the PLA-MSN sensor showed a unique "sieving" effect by regulating the rates of diffusion of the amino acid-based neurotransmitters into the sensor mesopores of the material.

An MCM-41 type mesoporous silica nanosphere-based (MSN) controlled-release delivery system has been synthesized and characterized using surface-derivatized cadmium sulfide (CdS) nanocrystals as *chemically removable caps* to encapsulate several

pharmaceutical drug molecules and neurotransmitters inside the organically functionalized MSN mesoporous framework. We studied the stimuli-responsive release profiles of vancomycin- and adenosine triphosphate (ATP)-loaded MSN delivery systems by using disulfide bond-reducing molecules, such as dithiothreitol (DTT) and mercaptoethanol (ME), as *release triggers*. The biocompatibility and delivery efficiency of the MSN system with neuroglial cells (astrocytes) in vitro were demonstrated. In contrast to many current delivery systems, the molecules of interest were encapsulated inside the porous framework of the MSN not by adsorption or sol-gel types of entrapment but by capping the openings of the mesoporous channels with size-defined CdS nanoparticles to physically block the drugs/neurotransmitters of certain sizes from leaching out. We envision that this new MSN system could play a significant role in developing new generations of site-selective, controlled-release delivery nanodevices.

For reaching and repairing a damaged cell or for killing a cancer cell, a drug molecule -- no matter how potent -- has to enter the particular cell. Several carriers have been imagined and designed to facilitate the membrane penetration -- all suffering from laborious synthesis and the requirement of highly specific targeting. However, for many applications such as local cancer therapy or in vitro gene transfection, an ideal carrier will be able to penetrate any type of cell and deliver the encapsulated molecule inside the cell body.

We have recently developed a new mesoporous silica nanosphere-based (MSN) transmembrane carrier that demonstrates ability to effectively transport molecules of interest through various cell membranes via endocytosis. Our system took advantage of the ordered mesoporous structure of MSN, where the nanometer-sized pores are large enough to accommodate/encapsulate pharmaceutical drugs and neurotransmitters.¹ The drug-loaded

mesopores were covalently capped in situ with either surface derivatized CdS nanocrystals or polyamido amine (PAMAM) dendrimers through a chemically cleavable linkage. The removable caps prevented the mesopore-encapsulated molecules from leaching. As a proof of principle, we studied the transmembrane activity of MSNs loaded with membrane impermeable fluorescent dyes on HeLa human cancer cell line, rat neuronal cells, and CHO cell line. The confocal fluorescence images, TEM micrographs, and flow-cytometer measurements showed that the MSNs were successfully engulfed by the cells without exhibiting cytotoxicity or mitosis blockage.

In the same context, as the ability to penetrate the cell membrane was demonstrated, we tried our system as gene carrier. The plasmid DNA of choice was pEGFP – encoding Green Fluorescent Protein. We successfully achieved Green Fluorescent Protein (GFP) gene expression in HeLa human cancer cell line and rat neuronal cells. Attached we present a collection of images illustrating the engulfed fluorescent silica in the cell body (the nuclei of the cells were blue stained).

CHAPTER 1. GENERAL INTRODUCTION

Introduction and Dissertation Organization

The overall objective of this dissertation is to present the versatility of mesoporous silica nanomaterials for several applications described herein.

The dissertation is organized in eight chapters: the first chapter encloses a literature review, the chapters 2-8 consist of journal articles either published or submitted for publication and chapter 9 concludes this dissertation with summaries of the results and an outlook for future work.

Chapter 1 is an overview of nanostructured mesoporous sol-gel materials with emphasis on their application in catalysis, sensing and biology.

Chapter 2 presents a new method for fine tuning the amount of accessible functional groups on the internal surface of the mesopores in Mesoporous Silica Nanospheres (MSN). We developed a synthetic method that can fine tune the amount of chemically accessible organic functional groups on the pores surface of Mesoporous Silica Nanospheres (MSN). The principle of this method resides on exploiting electrostatic and size matching between the cationic alkylammonium head group of the CTAB surfactant with various anionic organoalkoxysilane precursors at the micelle-water interface in a base-catalyzed condensation reaction of silicate (a journal article accepted for publication). My personal contribution represents 55% of the presented research.

Chapter 3 describes the application of mesoporous silica nanomaterials in two catalysis applications. We demonstrated that a homogeneous coverage of mesopores with organic functional groups can be achieved through rational design/choice of organosilane

precursors. By employing an ethylenediamine functional group for chelating Cu^{2+} , a Cu-functionalized MSNs silica catalyst was used for the synthesis of polyalkynylene-based conducting polymer (molecular wire). My personal contribution represents 50% of the presented research.

Chapter 4 outlines the organically functionalized MSN for another catalytic application. Organosulfonic acid-functionalized mesoporous silicas were synthesized in a one-step approach of co-condensing inorganic-organic reagents in the presence of different surfactant templates with in situ oxidation of the thiol groups to the sulfonic acid groups. The resulting materials were tested for their catalytic performance in the esterification of fatty acid with methanol to produce methyl esters. The activity of the organosulfonic acid-functionalized silicas in the esterification was compared to that of standard acidic resins. (published journal articles). My personal contribution represents 30% of the presented research.

Chapter 5 presents a sensing application of Mesoporous Silica Nanospheres (MSNs). We have synthesized a poly(lactic acid) coated mesoporous silica nanosphere (PLA-MSN) material that can serve as a fluorescence sensor system for detection of amino-containing neurotransmitters in neutral aqueous buffer. We investigated the molecular recognition events between several structurally simple neurotransmitters, i.e., dopamine, tyrosine, and glutamic acid and a pore surface-anchored o-phthalic hemithioacetal (OPTA) group, which functions as a fluorescence-sensing group that can react with the neurotransmitters with primary amine groups and form the corresponding fluorescent isoindole products. The poly(lactic acid) layer of the PLA-MSN sensor showed a unique "sieving" effect that regulates the rates of diffusion of the amino acid-based neurotransmitters into the sensor

mesopores of the material (published journal article). My personal contribution represents 51% of the presented research.

Chapter 6 is focused on the application of MSNs in drug delivery. The mesoporosity of MSNs confer these materials properties of a sponge: they can soak impressive amounts of molecules in solution. However, the cannels being both-ends opened, the content is easily leaching. Consequently, we have developed a “capping” strategy. We examined bio-friendly molecules such as polyamidoamine dendrimers of generations G2.5 to G4.5 as the caps. The release profiles of the different capped MSNs were investigated. My personal contribution represents 20% of the presented research.

In Chapter 7 the drug delivery system employed MSNs loaded with Doxorubicin, an anticancer drug. The results demonstrated that these nano-Trojan horses have ability to deliver Doxorubicin to cancer cells and induce their apoptosis (submitted journal articles). My personal contribution represents 50% of the presented research.

Chapter 8 is devoted to the development of a gene transfection nanocarrier that has MSNs as a core of the nanocomposite. We exploited not only the mesopores but also the surface and the silica matrix of these beads for biological applications. A multi-functionalized, MSN-based transfection vector with G2-PAMAM dendrimers covalently attached to MSNs exterior surface was synthesized. The p-EGFP-C1 gene-coated MSN nanocomposite was able to transfect cancer cell lines, such as human HeLa and CHO cancer cell lines. The green fluorescent protein expression induced by the MSN system in these cells was monitored via fluorescent microscopy and confocal laser microscopy. The results indicated that the transfected cells exhibited less or none of the cytotoxicity commonly associated with the use other transfection methods. The gene carrier potential of MSNs by in

transfecting primary cells and cotransfecting of two different genes was also investigated. My personal contribution represents 49% of the presented research.

The results indicated the versatility of this novel gene carrier for rationally designed gene therapy (published and submitted journal articles).

Finally, Chapter 9 is a brief conclusion of the dissertation with a general assessment of the accomplished goals as well as an overview of potential future applications.

Literature Review

Several versatile surfactant templated sol-gel pathways have been developed to prepare nanostructured porous materials and composites with different morphologies (e.g., monoliths, nanospheres, nanoparticles, and thin films), structures, compositions and properties. The synthetic conditions were systematically studied and optimized. The template effects on pore structure as well as synthetic process, especially template removal steps as well as the systematic functionalization, have been investigated.¹⁻⁴

In the early nineties,^{1(a)} scientists from *Mobil Oil Corporation* synthesized ordered mesoporous materials of the M41S type, MCM-41 being one of the distinguished members of this family.

In M41S materials, a liquid crystal templating (LCT) mechanism is a process during which long chain surfactant molecules arrange themselves through micelle self-assembly to form liquid-crystalline phases, surrounded by inorganic oxides forming a framework to generate the formation of hexagonal, lamellar or cubic structures, as illustrated in Figure I-1.

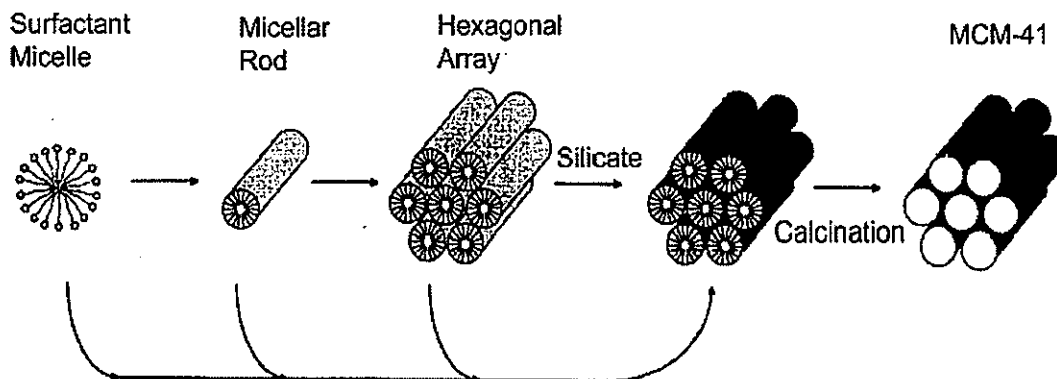


Figure 1-1. Schematics of MCM-41 type materials formation mechanism

This material possesses a porous system consisting of hexagonally arranged channels with diameters varying from 15 to 100 Å. MCM-41 has attracted the attention of scientists due to its elevated specific surface area, high thermal and hydrothermal stability, possibility of controlling its pore size and its hydrophobicity and acidity.

Also, recent advancements in utilizing organic surfactants or block copolymers as structure-directing templates for the syntheses of structurally well-defined mesoporous silica materials, such as MCM-48,^{1(b)} SBA-15,² MSU,³ and FSM-16,⁴ has attracted much attention for their potential applications in sensing,⁵ catalysis,⁶ and drug delivery.⁷ Obviously, the realization of these applications greatly depends on the ability of functionalization of the interior and exterior surfaces of the mesoporous silicas with various organic functional groups.

Although a wide variety of synthetic approaches have been pursued and some significant progresses have been made, few would argue that the current state-of-the-art methods, such as post synthesis grafting⁸ and organosiloxane/siloxane co-condensation

methods,⁹ need not to be improved in terms of controlling the amount and location of the incorporated functional groups on the surface of the mesoporous silica materials. For example, functional groups incorporated via the post synthesis grafting method typically congregate at the opening parts of porous channels resulting in an inhomogeneous surface coverage,¹⁰ whereas the amount of functional groups introduced by the organosiloxane/siloxane co-condensation method is yet to reach above 25% surface coverage without reaching an uniform coverage.

The composition and pore structures were thoroughly studied with various spectroscopic and microscopic methods such as IR, TGA, SEM, TEM, BET (gas sorption measurements), XRD and solid state NMR.

As part of one of the most active research areas in science, nanoscience,¹¹ these materials has also raised great interest in the fields of microscale electronics,¹²⁻¹⁴ electro-optics,¹⁵ biosensors,¹⁶⁻¹⁸ etc. One particularly interesting application is the development of novel nanomaterials-based drug delivery systems. Traditionally, responsive polymer systems have been employed in such devices.¹⁹⁻²⁰ For example, degradable polymers are synthesized in the presence of the drug molecule of interest.²¹ The resulting polymer/drug composite materials usually exhibit slow rates of drug release under normal conditions. Upon stimulation, the degradation of polymer matrix is accelerated, and the release of drug molecules is thereby enhanced. Drug delivery polymers that are responsive toward several types of stimulants, such as temperature, pH, and magnetic/electric field, have been reported in the literature.²²⁻²⁵

In addition to polymer-based drug delivery systems, the organically functionalized MCM-type mesoporous silica materials²⁶⁻²⁷ offer several attractive features, such as stable

mesoporous structures, large surface areas, tunable pore sizes and volumes, and well-defined surface properties, that are ideal for encapsulation of pharmaceutical drugs, proteins,²⁸⁻³² and other biogenic molecules.³³

Few approaches reported in literature have utilized solid silica nanoparticles as gene transfection vectors or enhancers.³⁴⁻³⁵ However, there are no precedent reports for utilization of mesoporous silica-based material in intracellular gene transfer. The two publications related to intracellular delivery: drug delivery and gene transfection have brought a new dimension to the applicability of MSNs. Virtually any drug within a size range compatible with the size of the meso-channels has potential to be encapsulated and further deliver intracellularly. In the same way, large polymeric molecules such as DNA and RNA that have ability to be electrostatically attached to the derivatized-MSN are delivered to cells.

In conclusion, mesoporous silica materials proved versatility in several applications, as will be showed in the current dissertation.

References

- (1) (a) C. T. Kresge, M. E. Leonowicz, W. J. Roth, J. C. Vartuli, and J. S. Beck, *Nature (London)*, **1992**, 359, 710 ; (b) Beck, J.S.; Vartuli, J.C.; Leonowicz, M.E.; Kresge, C.T.; Schmitt, K.D.; Chu, C.T.W.; Olson, D.H.; Sheppard, E.W.; McCullen, S.B.; Higgins, J.B.; Schlenker, J.L. *J. Am. Chem. Soc.*, **1992**, 114, 10834.
- (2) D. Zhao, J. Feng, Q. Huo, N. Melosh, G. H. Frederickson, B. F. Chmelka, and G. D. Stucky, *Science (Washington, D. C.)*, **1998**, 279, 548.
- (3) S. A. Bagshaw, E. Prouzet, and T. J. Pinnavaia, *Science (Washington, D. C.)*, **1995**, 269, 1242.

- (4) S. Inagaki, A. Koiwai, N. Suzuki, Y. Fukushima, and K. Kuroda, *Bull. Chem. Soc. Jpn.*, **1996**, *69*, 1449.
- (5) (a) V. S. Y. Lin, C.-Y. Lai, J. Huang, S.-A. Song, and S. Xu, *J. Am. Chem. Soc.*, **2001**, *123*, 11510. (b) D. R. Radu, C.-Y. Lai, J. W. Wiench, M. Pruski, and V. S. Y. Lin, *J. Am. Chem. Soc.*, **2004**, *126*, 1640.
- (6) (a) S. Huh, H.-T. Chen, J. W. Wiench, M. Pruski, and V. S. Y. Lin, *J. Am. Chem. Soc.*, **2004**, *126*, 1010. (b) A. Corma, *Chem. Rev.*, **1997**, *97*, 2373. (c) J. M. Thomas, *J. Mol. Catal. A*, **1999**, *146*, 77. (e) D. Brunel, A. C. Blanc, A. Galarneau, and F. Fajula, *Catal. Today*, **2002**, *73*, 139, and references therein.
- (7) (a) C.-Y. Lai, B. G. Trewyn, D. M. Jeftinija, K. Jeftinija, S. Xu, S. Jeftinija, and V. S. Y. Lin, *J. Am. Chem. Soc.*, **2003**, *125*, 4451. (b) N. K. Mal, M. Fujiwara, Y. Tanaka, T. Taguchi, and M. Matsukata, *Chem. Mater.*, **2003**, *15*, 3385.
- (8) J. Liu, Y. Shin, Z. Nie, J. H. Chang, L.-Q. Wang, G. E. Fryxell, W. D. Samuels, and G. J. Exarhos, *J. Phys. Chem. A*, **2000**, *104*, 8328, and references therein.
- (9) A. Stein, B. J. Melde, and R. C. Schroden, *Adv. Mater. (Weinheim, Ger.)*, **2000**, *12*, 1403, and references therein.
- (10) M. H. Lim and A. Stein, *Chem. Mater.*, **1999**, *11*, 3285.
- (11) Wilson, M.; Kannangara, K.; Smith, G.; Simmons, M.; Raguse, B. *Nanotechnology: Basic Science and Emerging Technologies*; Chapman and Hall/CRC: Boca Raton, FL, **2002**.
- (12) Macucci, M.; Iannaccone, G.; Greer, J.; Martorell, J.; Sprung, D. W. L.; Schenk, A.; Yakimenko, I. I.; Berggren, K.-F.; Stokbro, K.; Gippius, N. *Nanotechnology* **2001**, *12*, 136.

- (13) Dai, L. In *Perspectives of Fullerene Nanotechnology*; Osawa, E., Ed.; Kluwer Academic Publishers: Dordrecht, Netherlands, **2002**.
- (14) Allan, G.; Delerue, C.; Krzeminski, C.; Lannoo, M. In *Nanostructured Materials*; Knauth, P., Schoonman, J., Eds.; Kluwer Academic Publishers: Norwell, MA, 2002, pp 161.
- (15) Krenn, J. R. *Nature Mater.* **2003**, *2*, 210.
- (16) Cullum, B. M.; Vo-Dinh, T. *Biomedical Photonics Handwork*; CRC Press LLC: Boca Raton, FL, **2003**.
- (17) Lin, V. S. Y.; Lai, C.-Y.; Huang, J.; Song, S.-A.; Xu, S. *J. Am. Chem. Soc.* **2001**, *123*, 11510.
- (18) Livage, J.; Coradin, T.; Roux, C. *J. Phys.: Condensed Matter* **2001**, *13*, R673.
- (19) Uhrich, K. E.; Cannizzaro, S. M.; Langer, R. S.; Shakesheff, K. M. *Chem. Rev.* **1999**, *99*, 3181.
- (20) Langer, R. *Acc. Chem. Res.* **1993**, *26*, 537.
- (21) Li, Y.; Kissel, T. *J. Controlled Release* **1993**, *27*, 247.
- (22) Peppas, N. A.; Huang, Y.; Torres-Lugo, M.; Ward, J. H.; Zhang, J. *Annu. Rev. Biomed. Eng.* **2000**, *2*, 9.
- (23) Kost, J.; Langer, R. *Adv. Drug Delivery Rev.* **2001**, *46*, 125.
- (24) Ishihara, K.; Kobayashi, M.; Ishimaru, N.; Shonohara, I. *Polym. J.* **1984**, *16*, 625.
- (25) Fischel-Ghodsian, F.; Brown, L.; Mathiowitz, E.; Brandenburg, D.; Langer, R. *Proc. Natl. Acad. Sci. U.S.A.* **1988**, *85*, 2403.
- (26) Stein, A.; Melde, B. J.; Schroden, R. C. *Adv. Mater. (Weinheim, Germany)* **2000**, *12*, 1403.

- (27) Sayari, A.; Hamoudi, S. *Chem. Mater.* **2001**, *13*, 3151.
- (28) Vallet-Regi, M.; Ramila, A.; del Real, R. P.; Perez-Pariente, J. *Chem. Mater.* **2001**, *13*, 308.
- (29) Munoz, B.; Ramila, A.; Perez-Pariente, J.; Diaz, I.; Vallet-Regi, M. *Chem. Mater.* **2003**, *15*, 500.
- (30) Ramila, A.; Munoz, B.; Perez-Pariente, J.; Vallet-Regi, M. *J. Sol.-Gel Sci. Technol.* **2003**, *26*, 1199.
- (31) Mal, N. K.; Fujiwara, M.; Tanaka, Y.; Taguchi, T.; Matsukata, M. *Chem. Mater.* **2003**, *15*, 3385.
- (32) Diaz, J. F.; Balkus, K. J., Jr. *J. Mol. Catal. B: Enzymatic* **1996**, *2*, 115.
- (33) Han, Y.-J.; Stucky, G. D.; Butler, A. J. *Am. Chem. Soc.* **1999**, *121*, 9897.
- (34) Kisler, J. M.; Stevens, G. W.; O'Connor, A. J. *Mater. Phys. Mech.* **2001**, *4*, 89.
- (35) Luo, D.; Saltzman, W. M. *Nature Biotech.* **2000**, *18*, 893

CHAPTER 2. FINE-TUNING THE DEGREE OF ORGANIC FUNCTIONALIZATION OF
MESOPOROUS SILICA NANOSPHERE MATERIALS VIA AN INTERFACIALLY
DESIGNED CO-CONDENSATION METHOD

A paper accepted for publication in *Chemical Communications*

Daniela R. Radu, Cheng-Yu Lai, Jianguo Huang, Xu Shu, Victor S.-Y. Lin

Department of Chemistry, Iowa State University, Ames, Iowa

Abstract

A synthetic method that enables the fine tuning of the amount of chemically accessible organic functional groups on the pore surface of MCM-41 type mesoporous silica nanosphere (MSN) materials has been developed by electrostatically matching various anionic organoalkoxysilanes with the cationic cetyltrimethylammonium bromide micelles in a base-catalyzed condensation reaction of tetraethoxysilane.

Introduction

Recent advancements in utilizing organic surfactants or block copolymers as structure-directing templates for the syntheses of structurally well-defined mesoporous silica materials, such as MCM-41/48,¹ SBA-15,² MSU-n,³ and FSM-16,⁴ has attracted much attention for their potential applications in sensing,⁵ catalysis,⁶ and drug delivery.⁷ Obviously, the realization of these applications greatly depends on the ability of functionalization of the interior and exterior surfaces of the mesoporous silicas with various

organic functional groups. Although a wide variety of synthetic approaches have been pursued and some significant progresses have been made, few would argue that the current state-of-the-art methods, such as *post synthesis grafting*⁸ and *organosiloxane/siloxane co-condensation*⁹ methods, need to be improved in terms of controlling the amount and location of the incorporated functional groups on the surface of the mesoporous silica materials. For example, functional groups incorporated via the *post synthesis grafting* method typically congregate at the opening parts of porous channels resulting in an inhomogeneous surface coverage,¹⁰ whereas the amount of functional groups introduced by the *organosiloxane/siloxane co-condensation* method is yet to reach above 25% surface coverage without destroying the structural integrity and the long-range periodicity of the synthesized materials.^{9,10} Herein, we report on a new co-condensation method that could generate organically functionalized, MCM-41 type of mesoporous silica nanosphere materials while controlling the surface concentration of organic functional groups.

Materials and Methods

1. Materials

3-Mercaptopropionic acid (99+%), 2,2'-dipyridyl disulfide (98%), (3-mercaptopropyl)trimethoxysilane (MPTES) (95%), 2-mercaptoethanesulfonic acid sodium salt (98%), cetyltrimethylammonium bromide (CTAB), tetraethyl orthosilicate (TEOS, 96%) and dithiothreitol (DTT) were purchased from Aldrich Chemical Co. (Milwaukee, WI). Acetic acid (Glacial), hydrochloric acid (37.4%), sodium hydroxide, ethanol (anhydrous), methanol (HPLC grade), tetrahydrofuran (HPLC grade), hexanes (pesticide grade) and ethyl ether (anhydrous) were obtained from Fisher Scientific Co. (Pittsburgh, PA). Nanopure water

was deionized to 18.0 M Ω -cm in a Barnstead E-pure water purification system and used for the synthesis of MSN materials.

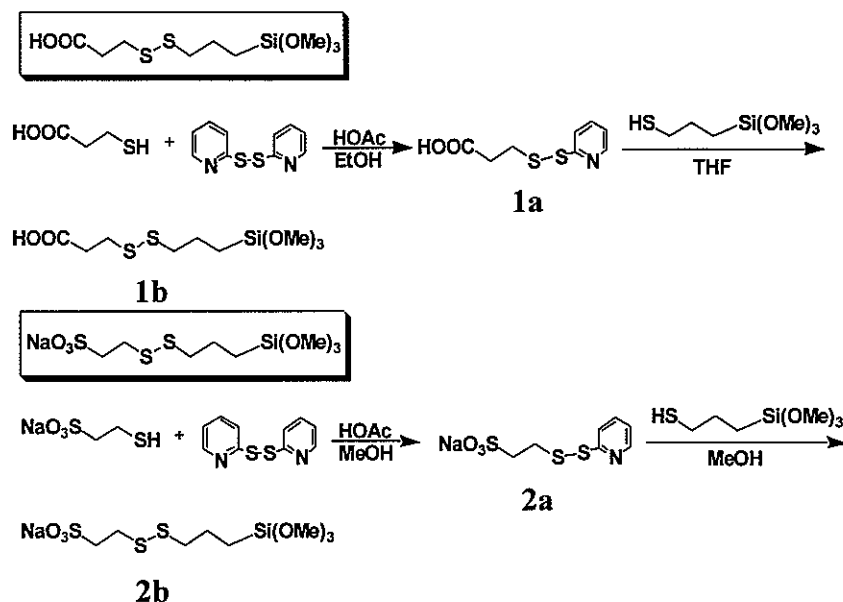


Figure 2-1. Schematic representation of the synthesis of organoalkoxysilane precursors

2. Synthesis of organoalkoxysilane precursors

2.1 Synthesis of 2-[3-(trimethoxysilyl)-propyl]disulfanyl-propionic acid (1b)

As depicted in Figure 2-1, 2-Carboxyethyl-2-pyridyl-disulfide, compound (1a), was prepared according to a procedure published by Carlsson.¹⁴ In a typical synthesis, 3.75 g (17 mmol) of 2,2'-dipyridyl disulfide (Aldrithiol-2) was dissolved in 30 mL of ethanol and a solution of 0.87 mL of mercaptopropionic acid in 5 mL ethanol was injected dropwise. After 20 h of stirring at room temperature, the crude yellow oil product was isolated by rotary evaporation. The purified product (1.45 g, yield = 40%) was obtained from an alumina column chromatography (eluent = CH₂Cl₂/EtOH 3:2 v/v). The product 1.45 g (6.8 mmol) is

corresponding to 40% yield. The characterization of compound 1a is consistent with the literature reported data.¹⁴

2-[3-(trimethoxysilyl)-propyldisulfanyl]-propionic acid, compound (1b), was prepared by dissolving compound 1a (1.51 g, 7 mmol) in 30 mL THF, followed by a dropwise addition of MPTMS (1.1 g, 5.6 mmol). The resulting yellow solution was stirred under N₂ atmosphere for 12 h. After flash evaporation of the solvent, the yellow product was purified by silicagel column chromatography using EA/ hexane in 1:2 ratio as eluent. The purified product (1 g) was isolated with a 60% yield. ¹H-NMR (CDCl₃), δ 0.76 (t, 2H, CH₂(1)), 1.81 (q, 2H, CH₂(2)), 2.71 (t, 2H, CH₂(5)), 2.81 (t, 2H, CH₂(3)), 2.91 (t, 2H, CH₂(4)), 3.60 (s, 1H, OCH₃); ¹³C-NMR (D₂O), δ 10.25, 13.69, 23.75, 34.83, 36.98, 42.26, 180.99.

2.2 Synthesis 2-[3-(trimethoxysilyl)-propyldisulfanyl]-ethanesulfonic acid, (2b)

As depicted in Fig. 2-1, 2,2'-dipyridyl disulfide (8.82 g, 40.0 mmol) was dissolved in 50.0 mL methanol, followed by an addition of 1.6 mL of glacial acetic acid as catalyst. To this mixture, 2-mercaptoethanesulfonic acid sodium salt (3.82 g, 20.0 mmol) in 30.0 mL methanol was added dropwise in 30 min with stirring. The reaction mixture was protected from light and stirred at room temperature overnight, followed by solvent evaporation under vacuum. The crude product was purified by dissolving in a small amount of methanol, followed by recrystallization in ethyl ether and dried under vacuum to yield compound 2a (5.14 g, yield = 94.0%). ¹H-NMR (300 MHz; DMSO-d₆), δ 2.73 (m, 2H, CH₂), 3.02 (m, 2H, CH₂), 7.24 (d, 1H, ArH), 7.81 (m, 2H, ArH), 8.45 (d, 1H, ArH).

To synthesize 2-[3-(trimethoxysilyl)-propyldisulfanyl]-ethanesulfonic acid sodium salt (2b), compound 2a (1.36 g, 5.0 mmol) was dissolved in 20.0 mL of methanol with 1.0 mL of glacial acetic acid. To this mixture, (3-mercaptopropyl) trimethoxysilane (0.95 mL,

5.0 mmol) in 10.0 mL of methanol was added dropwise. The mixture was protected from light and stirred under nitrogen at room temperature overnight. The reaction was quenched and the solvent was evaporated under vacuum. The solid product was dissolved in a small amount of methanol, followed by ethyl ether precipitation. The purified product (5.14 g, yield = 74.7%) was collected by filtration and dried under vacuum. $^1\text{H-NMR}$ (300 MHz; D_2O) δ 0.79 (*t*, 2H, $\text{CH}_2(1)$), 1.83 (*q*, 2H, $\text{CH}_2(2)$), 2.81 (*t*, 2H, $\text{CH}_2(3)$), 3.03 (*t*, 2H, $\text{CH}_2(5)$), 3.27 (*t*, 2H, $\text{CH}_2(4)$), 3.60 (*s*, 7H, OCH_3).

3. Synthesis of MSN materials

Three organically functionalized mesoporous silica materials, MSN-COOH, MSN-SO₃H, and MSN-SH, were prepared by adding an ethanolic solution (2 mL, 2.24 mmol) of CDSP-TMS, SDSP-TMS, and the commercially available MP-TMS, respectively, to an aqueous solution (480 mL) of CTAB (2.74 mmol), NaOH (7.00 mmol), and TEOS (22.40 mmol) at 80°C. The reaction mixture was stirred for 2 h. The solid products were isolated by filtration and washed thoroughly with methanol. The surfactant-removed materials were obtained by refluxing 1 g of the MSN material in 170 mL of methanolic solution of HCl (1 M) for 12 h. The resulting surfactant-removed material was isolated by filtration, washed extensively with methanol, and dried under vacuum. To obtain mesoporous silica material with free thiol groups, the surfactant extracted MSN material was added to 100.0 mL of 5% NaHCO₃ (aq) containing a disulfide reducing agent, dithiothreitol (DTT) (1.88 g, 12.2 mmol). The mixture was stirred at room temperature for 4 h. The white product was then filtered and washed with water and methanol, following by vacuum drying.

4. Characterization of the Organic Functionalization of the MSN Materials

4.1 Powder XRD

Powder XRD diffraction patterns of MSN-COOH, MSN-SO₃H, and MSN-SH are summarized in Table 2-1. The data were collected on a Scintag XRD 2000 X-Ray diffractometer using Cu K α radiation. Low angle diffraction with a 2θ range of 1 to 10° was used to investigate the long-range order of the materials.

4.2 Nitrogen Sorption Analysis

Surface area (SA) and Median Pore Diameter (MPD) were measured using a Micromeritics ASAP2000 sorptometer. Samples were degassed at 90 °C for 1 h and at 150 °C for 4 h. Nitrogen adsorption and desorption isotherms of the MSN materials were obtained at -196 °C. Specific surface areas and pore size distributions were calculated using the Brunauer-Emmett-Teller (BET) and Barrett-Joyner-Halenda (BJH) method, respectively.

4.3 Scanning Electron Microscopy

Particle morphology of these MSN materials was determined by scanning electron microscopy (SEM) using a JEOL 840A scanning electron microscope with 10 kV accelerating voltage and 0.005 nA of beam current for imaging. For obtaining the transmission electron microscopy (TEM) micrograph displayed in the main text, a small aliquot was taken from a suspension of MSN in methanol, and placed in a lacey carbon-coated TEM grid, which was pulled through the suspension and allowed to dry in air. The specimen was given no further treatment, as it appeared stable under beam bombardment.

4.4 Thermogravimetric Analysis

TGA curves were recorded using a TA Instruments TGA 2950 thermogravimetric analyzer with a temperature ramp of 5 °C/min under continuous flow of nitrogen (100

mL/min). The percentage of weight loss when heating the samples of MSNs in the range of 1-1000°C is concluded in Table 2-2. In general, three or four distinct weight loss TGA profiles were found, including methanol, organic functional groups, and a small weight loss due to the dehydration of the surface hydroxyl groups.

4.5 ^{13}C Solid State NMR

The ^{13}C spectra shown in the Figure. 2-5 confirm the presence of the three organic functional groups in the MSN materials before the disulfide bond reductions. Solid-state ^{13}C CP-MAS NMR spectra were obtained at 75.47 MHz on a Bruker MSL300 spectrometer equipped with Bruker 4 mm rotor MAS probe. Magic-angle sample spinning rate was maintained at 10 KHz. The NMR spectra consisted of between 2,000 and 6,000 acquisitions with cross polarization times of 3 ms and pulse repetition times of 15 s. All chemical shifts reported are referenced to liquid SiMe_4 (TMS).

5. Quantification of chemically accessible surface-functionalized thiol coverage.

All experiments were performed in triplicate, by reacting a predetermined amount of material (in the range of 20 to 25 mg) with a methanolic solution of excess 2, 2'-dipyridyl disulfide (44 mg, 0.2 mmol dissolved in 5 mL methanol).

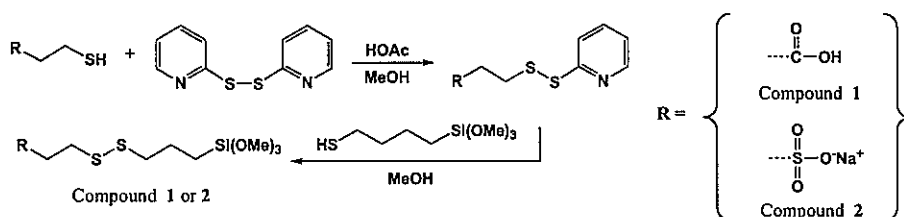
Results and Discussion

Our method involves the utilization of disulfide-containing organotrimethoxysilanes that have different anionic functional groups, such as 3-(3'-(trimethoxysilyl)-propyl-disulfanyl)-propionic acid (CDSP-TMS), 2-[3-(trimethoxy-silyl)-propyl-disulfanyl]-ethanesulfonic acid sodium salt (SDSP-TMS), and mercaptopropyl-trimethoxysilane (MP-

TMS), to electrostatically match with cationic cetyltrimethylammonium bromide (CTAB) surfactant micelles in a NaOH-catalyzed condensation reaction of tetraethoxysilane (TEOS) as shown in Figure 2-2. We were inspired by the recent reports by Larsen and Magid,¹¹ where they observed the anionic lyotropic series (citrate < CO₃²⁻ < SO₄²⁻ < CH₃CO₂⁻ < F⁻ < OH⁻ < HCO₂⁻ < Cl⁻ < NO₃⁻ < Br⁻ < CH₃C₆H₄SO₃⁻) for interaction with the CTAB surfactant micelle based on the enthalpy of transfer of the salt from water to solutions of 0.1 M CTAB. They concluded that anions less hydrated than Br⁻, such as sulfonate, will be able to replace Br⁻ and bind tightly to the cetyltrimethylammonium head group of the CTAB molecule thereby effectively mitigating the repulsion between these cationic head groups and stabilizing the micelle structure. Also, several recent reports¹² have also revealed that the long-range structure ordering of CTAB-templated mesoporous silicas could be improved by the additions of various anions. The tightly bound (less hydrated) anions, such as acetate and BF₄⁻, became incorporated in the silicate matrix due to their ability to compete with the silicate anions in displacing Br⁻ from the CTAB micelle.

In the present chapter, the different electrostatic matching effects of various anionic organoalkoxysilanes, such as thiolate-, carboxylate-, and sulfonate-containing organoalkoxysilanes, to CTAB micelles in governing the degree of organic functionalization of the MCM-41 type mesoporous silica materials are investigated.

Scheme 2-1.



First, two disulfide-containing organotrimethoxysilanes (CDSP-TMS and SDSP-TMS) with carboxylic and sulfonic acid groups, respectively, were synthesized via a synthetic approach outlined in Scheme 2-1. The two compounds were synthesized via a simple thiol activation of 3-mercaptopropionic acid and 2-mercaptoethanesulfonic acid sodium salt with 2,2'-dipyridyl disulfide followed by a disulfide exchange reaction with mercaptopropyltrimethoxysilane. Three organically functionalized mesoporous silica materials, MSN-COOH, MSN-SO₃H, and MSN-SH, were prepared by adding an ethanolic solution (2 mL, 2.24 mmol) of CDSP-TMS, SDSP-TMS, and the commercially available MP-TMS, respectively, to an aqueous solution (480 mL, 80 °C) of CTAB (2.74 mmol), NaOH (7.00 mmol), and TEOS (22.40 mmol, added at 80 °C prior to the addition of organoalkoxysilanes). The reaction mixture was stirred for 2 h. The solid products were isolated by filtration and washed thoroughly with methanol. Surfactant-removed materials were obtained with an acid extraction. All three materials exhibited spherical particle shape with an average particle diameter of 200 nm (Figure 2-2).

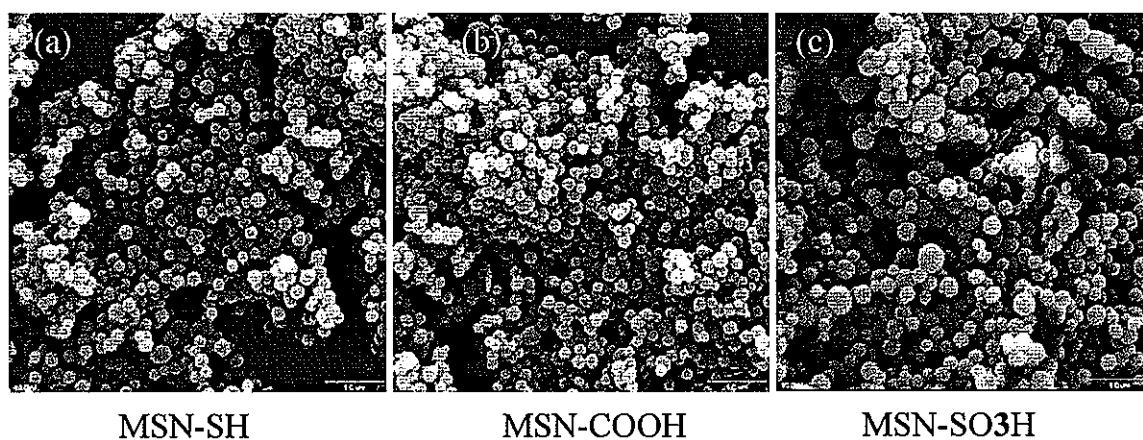


Figure 2-2. SEM images of MSN-SH (a), MSN-COOH (b) and MSN-SO₃H (c). All three materials exhibited spherical particle morphology, with an average particle diameter of 200 nm. All images are presented using the same magnification (scale bar = 1 μ m).

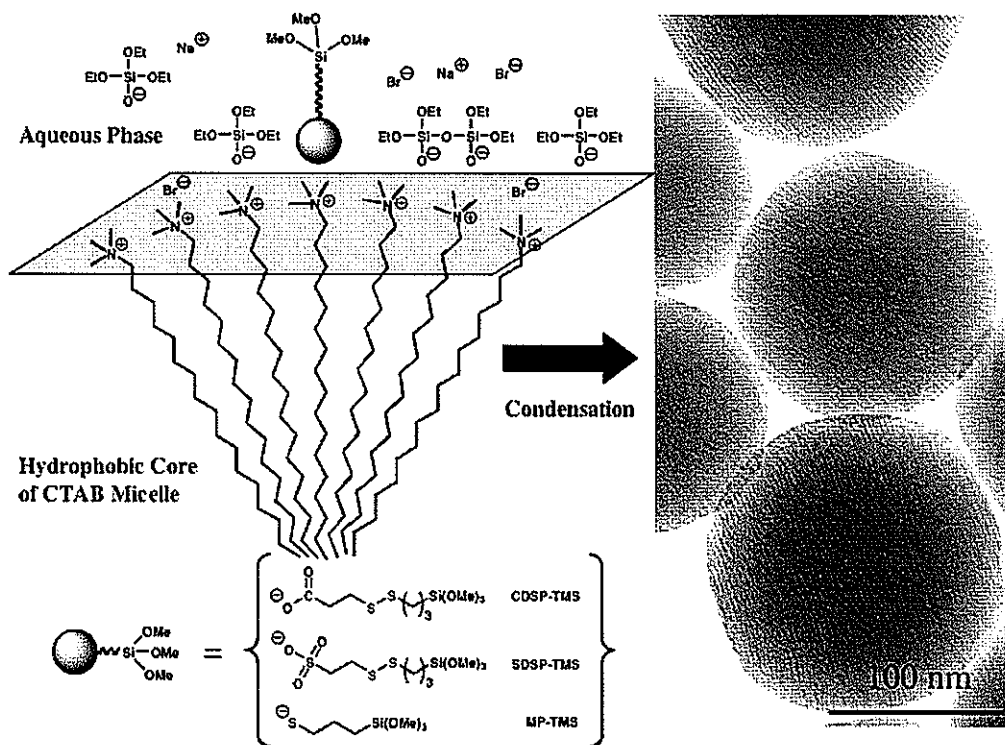


Figure 2-3. Schematic representation of the utilization of anionic organoalkoxysilane for controlling the functionalization of the MSN materials. The MCM-41 type mesoporous channels are illustrated by the parallel stripes shown in the TEM micrograph of the MSN-SH material.

The mesoporous structures of these organically functionalized MSN materials were determined by nitrogen adsorption-desorption surface analysis (BET isotherms and BJH pore size distributions), TEM, and powder X-ray diffraction (XRD) spectroscopy.

These materials exhibited diffraction patterns characteristic of hexagonal MCM-41 silicas, including (100), (110), and (200) peaks (Figure 2-3). In addition, all three MSN materials exhibited type IV BET isotherms with similar average BJH pore diameters (Figure 2-4 and Table 2-1). Hexagonally packed mesoporous channels were clearly observed in the TEM micrographs of these MSNs (Figure 2-1).

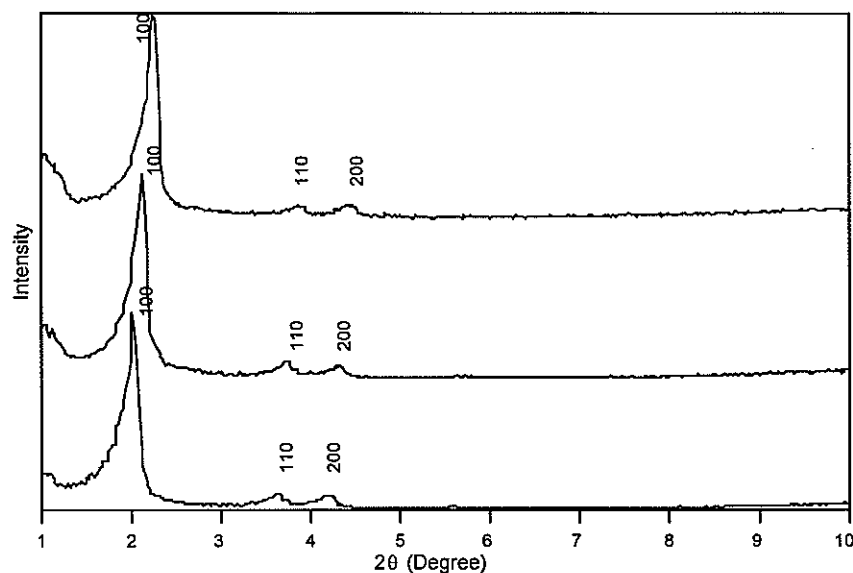


Figure 2-4. Powder XRD diffraction patterns of the MSN-SH (green), MSN-COOH (red) and MSN-SO₃H (blue) materials after treatment with disulfide reducing agent (DTT).

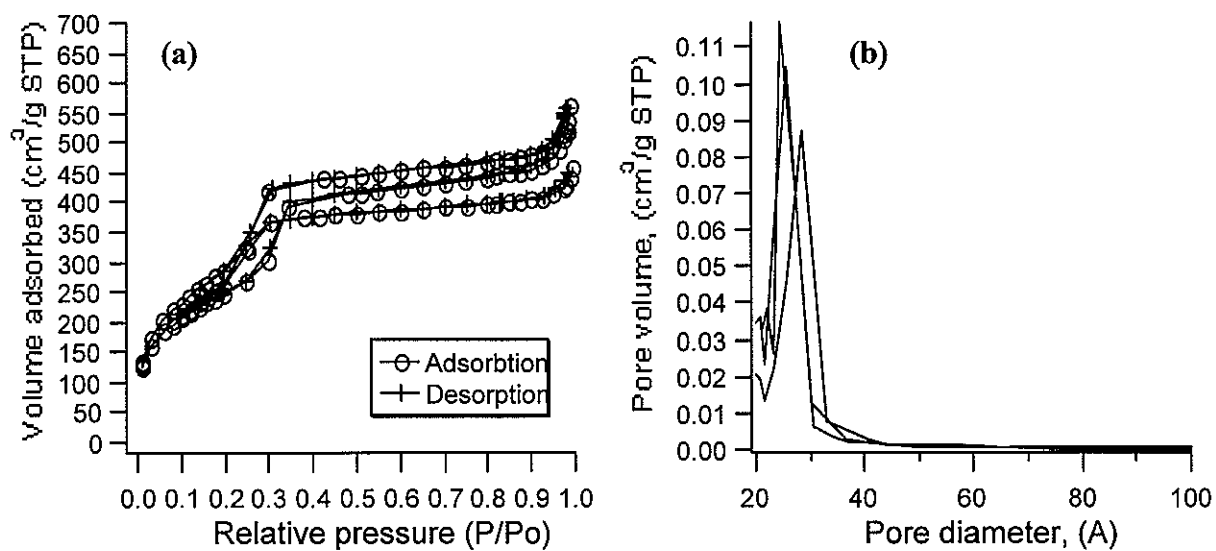


Figure 2-5. (a) Nitrogen sorption isotherms of the MSN-SH (green), MSN-COOH (red) and MSN-SO₃H (blue) materials after treatment with disulfide reducing agent (DTT). (b) Pore size distributions of the MSN-SH, MSN-COOH and MSN-SO₃H materials.

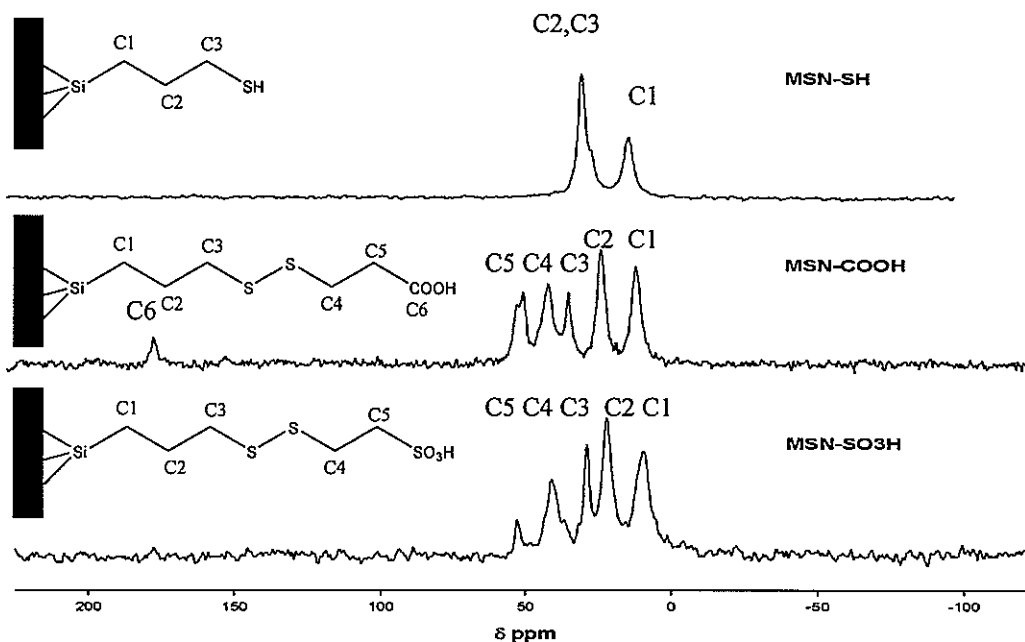


Figure 2-6. Solid state ¹³C CP-MAS NMR spectra of the MSN-SH (up), MSN-COOH (middle) and MSN-SO₃H (bottom).

The existence of the organic functional groups was confirmed by ¹³C solid state NMR spectroscopy (Figure 2-6).

Table 2-1. Structural properties of the organically functionalized MSN materials.

	Powder XRD			Nitrogen Sorption Isotherms		
	<i>d</i> ₁₀₀	<i>d</i> ₁₁₀	<i>d</i> ₂₀₀	surface area	pore volume	pore diameter
				(m ² /g)	(mL/g)	(Å)
MSN-SH	39.8	22.9	19.9	999	0.793	25.8
MSN-COOH	40.5	22.8	20.1	920	0.657	27.3
MSN-SO ₃ H	43.8	24.4	20.9	863	0.755	28.1

The nitrogen sorption isotherms of the three MSN materials exhibited a sharp step starting at ca. $p/p_0 = 0.38$, as shown in Figure 2-4a with reversible type IV isotherms. (The inflection

point is attributed to the commencement of pore filling from which the pore diameter can be roughly estimated).

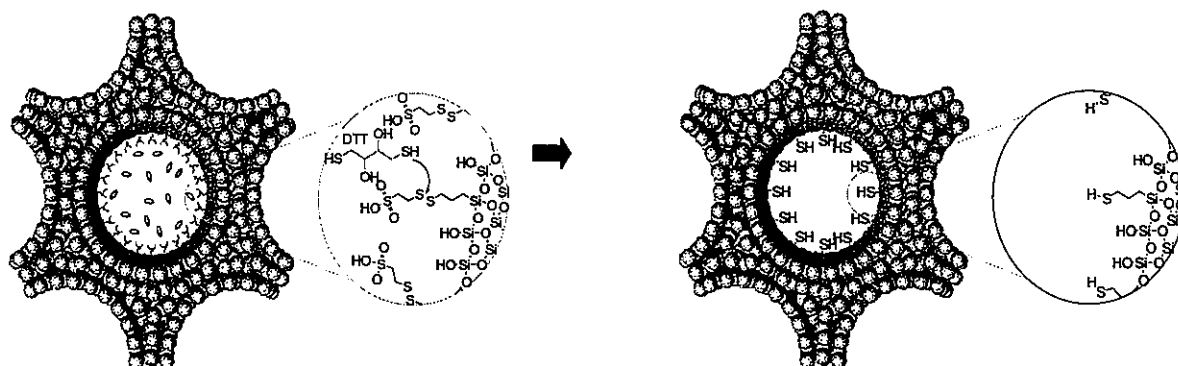


Figure 2-7. Schematic representation of the formation of thiol-functionalized mesoporous silica material (MSN-SO₃H) via disulfide reduction with dithiothreitol (DTT).

To quantify the amount of chemically accessible functional groups that are incorporated and oriented properly on the mesopore surfaces, we chemically converted the surface bound organic groups of the MSN-COOH and MSN-SO₃H materials to thiol (-SH) by treating them with a disulfide reducing agent, dithiothreitol (DTT) as depicted in Fig. 2-6.

As shown in Scheme 2-2, reactions of the resulting free thiol-functionalized materials with the 2,2'-dipyridyl disulfide gave rise to 2-pyridyldithio-derivatized surface functional groups along with a 2-pyridothione compound as the side product.

Scheme 2-2

